Indoor Performance Analysis of Genetically Optimized Circular Rotational Square Hyperboloid (GOCRSH) Concentrator

Daria Freier Raine[1,*], Firdaus Muhammad-Sukki[2,*], Roberto Ramirez-Iniguez[1], Tahseen Jafry[1] and Carlos Gamio[1]

[1] School of Computing, Engineering and Built Environment, Glasgow Caledonian University, 70 Cowcaddens Road, Glasgow, G4 0BA, United Kingdom

[2] School of Engineering & the Built Environment, Edinburgh Napier University, Merchiston Campus, 10 Colinton Road, Edinburgh EH10 5DT, Scotland, United Kingdom

* Corresponding author: daria_freier@outlook.de (D.F.R.); f.muhammadsukki@napier.ac.uk (F.M.-S.)

Abstract

In the past few years, there was an increasing popularity of portable solar chargers for providing access to clean affordable electricity to remote locations in developing countries. Looking at the surge in demand, it is also important to reduce the environmental impact of portable solar chargers. Solar photovoltaic (PV) concentrators have the potential to reduce the embodied energy and thus the embodied greenhouse gas emissions, human-toxicity and eco-toxicity potential during production, recycling and disposal stages of silicon PV solar panels. Yet, no solar PV concentrator designs have been proposed for portable solar systems for developing countries. Recently, a novel concentrator known as genetically optimized circular rotational square hyperboloid (GOCRSH) concentrator was developed to address this problem. This paper evaluates the performance of four types of GOCRSH concentrators; namely GOCRSH_A GOCRSH_B, GOCRSH_C$_{rh}$ and GOCRSH_D that have a geometrical gain of 3.73x, 3.34x, 3.80x and 4.07x respectively. The experimental analysis of these concentrators was performed indoors under standard test conditions, i.e. 1000 W/m^2, AM 1.5G and at a temperature of 25 ˚C to characterize the concentrators at normal incidence and to determine their angular response. Firstly, the fabrication process of the prototypes is described. Secondly, the GOCRSH concentrated devices and the reference cell are characterized at normal incidence, obtaining the current-voltage (*I-V*) and power-voltage (*P-V*) curves. Next, the angular response of the concentrators is obtained at various angles of incidence of up to ± 70° in increments of 5°. Mismatches between the simulation results and the experimental results are identified and possible error sources leading to the mismatch are discussed. Lastly, the increase in solar cell temperature under constant illumination and its impact on the solar cell performance is recorded for the GOCRSH_A concentrating device. From the indoor experiments, it was found that the prototypes were showing the maximum power point ratio under normal incidence of 2.9x, 2.6x, 3.9x and 2.7x with the GOCRSH_A GOCRSH_B, GOCRSH_C_{rh} and GOCRSH_D respectively.

Keywords: genetically optimized circular rotational square hyperboloid concentrator, solar photovoltaic, indoor performance analysis, opto-electronic gain.

1. Introduction.

The Sustainable Development Goals (SDGs) were agreed in 2015 by 193 nations to "mobilize efforts to end all forms of poverty, fight inequalities and tackle climate change, while ensuring that no one is left behind" (United Nations, 2021). Out of the 16 SDGs, Goal 7 "Access to affordable, reliable, sustainable and modern energy for all" (United Nations, 2017) is seen as an enabler to achieve the other fifteen goals (Scott et al., 2017). Yet, worldwide, over 1.1 billion people have no access to electricity. They therefore lack its basic commodity which is clean lighting (IEA, 2017). Alternative sources such as kerosene lamps, candles or burning switchgrass limit the ability of the affected people to study or work after sunset due to the poor quality of the light they produce. Furthermore, these light sources have associated health risks such as poisoning from the inhaled fumes, chronical lung diseases, eye irritation as well as increased potential for burns from accidental fires. These hazards mostly affect women and children since they are predominantly involved in household chores like cooking (Kimemia et al., 2014).

Approximately 80% of the affected people live in rural communities in developing countries (IEA, 2017; Scott et al., 2017). One of the main hurdles to electrifying rural areas is the lack of infrastructure. Many utility companies find it less desirable to build the required infrastructure due to low electricity demand, small population density and long distances to the nearest substation connecting remote communities. Additionally, the issue of theft of cables as well as other infrastructural materials and unreliable customer payments diminished the demand for centralized electricity supply (Avila et al., 2017).

It is however not the grid connection that people want, but the potential benefits the energy provides. This suggests that the way towards electrification does not need to be a centralized solution. Most of the world's energy poor live in sub-Saharan Africa, Asia and the Pacific and predominantly in areas with an abundance of solar radiation throughout the year (Abubakar Mas'ud et al., 2016; Beuse et al., 2020; Burke et al., 2019; Keane, 2014; Palit, 2013; Yan et al., 2019). Solar systems are therefore viewed as the way forward to decentralized electrification.

One of the most sought after technologies for electrification is the portable solar charger. This device is under continuous development aiming to achieve lower cost, faster battery charge and more electricity generation to prolong light hours at a high light intensity. The most commonly used PV materials in solar lights are monocrystalline and polycrystalline silicon due to their high conversion efficiencies (laboratory efficiency of 26.7% and 22.3% respectively (Green et al., 2018)), cell stability and no toxic components unlike Cadmium telluride (CdTe), Copper indium gallium (di)selenide (CIGS) and Gallium arsenide (GaAs) (Fthenakis, 2003). Yet, the production of silicon is energy intensive and has associated greenhouse gas (GHG) emissions (Vellini et al., 2017).

To reduce the environmental impact of solar lights, the use of solar photovoltaic concentrators is suggested. A solar concentrator focuses light rays from a large area onto a smaller area increasing the electrical output of the solar system (Muhammad-Sukki et al., 2014). The report published by the Fraunhofer Institute for Solar Energy Systems (2018) shows that the embodied energy per W_p can be reduced by using solar photovoltaic concentrating systems (Lamnatou et al., 2016).

In the past three decades, a large number of concentrator designs have been developed by researchers. For example, Sharma and Bhattacharya (2020) developed a static cylindrical Fresnel lens made from silicon glass. They established that their optimum concentrator design has the following parameters: 20 cm diameter of the cylindrical lens, 37° prism angle, a distance between the absorber and the concentrator axis of 11 cm and a 5 cm width of the absorber. From their simulation, they found that their optimum design is capable of increasing the energy collection by approximately 50%. Liu et al. (2017) studied a planar Lambertian reflector-based concentrator that has a geometrical concentration ratio of 2x. Their ray tracing analysis showed that an optical concentration gain of 1.29x can be achieved when compared to a non-concentrating counterpart.

Xuan et al. (2017) studied a concentrator known as asymmetric lens-walled compound parabolic concentrator (ALCPC). They carried out simulations to determine its optical performance by using the software Lighttools, and found that this design has a wide acceptance angle of ±60°. The outcome from their experiment results indicated that the ALCPC is capable of increasing the maximum power by a ratio of 1.74x when compared with a bare PV cell. Elminshawy et al. (2019) utilized a V-trough PV concentrator integrated with a buried water heat exchanger as to cool the CPV system. A prototype was developed and tested at Port Said, Egypt. The V-trough was constructed from 1 mm aluminium plate reflectors with dimensions of 1650 mm × 1000 mm. They found that the cooling system improved their CPV's peak generated electrical power by as high as 28.3% when compared with the ones without a cooling system. Li et al. (2019) tested a 3-D compound parabolic concentrator (CPC) and found that the CPC design achieved a maximum optical efficiency of 85.4% and a concentration gain of 4.1x when compared with a non-concentrating counterpart.

Meanwhile, Foster et al. (2020) evaluated the effect of diffuse radiation at the output of a rotationally asymmetrical compound parabolic concentrator (RACPC). The RACPC has a geometrical concentration gain of 3.67x, a total height of 3 cm and was fabricated from Polymethyl Methacrylate (PMMA). From their experiment, it was found that the RACPC design could achieve an opto-electronic gain of 2.20x under diffuse radiation when compared with a bare PV cell. Sarmah et al. (2014), on the other hand, carried out an indoor characterization of a linear dielectric compound parabolic concentrator (CPC). The CPC design has an acceptance angle range between 0° and 55°, a geometrical concentration gain of 2.8x and was fabricated from polyurethane. With the dielectric CPC design a maximum power ratio of 2.27x was demonstrated when compared to a similar non-concentrating PV cell. Baig et al. (2020) utilized a reversed truncated pyramid concentrator to increase the power output from a perovskite cell. From the experimental work, they found that the concentrator increased the power output from 1.88 mW to 15.88 mW – a factor of 8.4x.

Despite various concentrator designs, Freier et al. (2017) argued that these concentrators have not been used for portable solar systems. In order for a concentrator to be implemented in a portable solar systems, it must have the following characteristics: (i) it needs to have the same light acceptance angle on all vertical planes for easy use; (ii) it must have a sufficiently high concentration ratio to enable savings in photovoltaic material; (iii) it needs to have minimum height and volume to reduce weight and manufacturing cost, (iv) its design needs to be suitable for a concentrator array to be produced from a single mould to minimize manufacturing and assembly costs. They then developed a novel circular rotational square hyperboloid (CRSH) concentrator design. Based on the ray tracing analysis of the CRSH they concluded that a maximum optical concentration gain of 3.94x can be achieved. The CRSH was recently optimized using genetic algorithms, and the new design is known as genetically optimized circular rotational square hyperboloid (GOCRSH) concentrator (Freier Raine et al., 2020). Genetic algorithm is a probabilistic optimization algorithm that allows for a continuous search of an optimum or near- optimum solution (Cvijovic and Klinowski, 2002). The optimization offers several advantages including: (i) it allows a more compact concentrator design; (ii) it is easy to use; (iii) it has an optical concentration ratio of around 3x, and allows wide half-acceptance angles of ±40° which enables it to capture light for more than 5 hours without electromechanical tracking.

While a series of simulations have been carried out to identify the optimized GOCRSH concentrator, no experimental work has been carried out to evaluate its electrical performance. The aim of this paper is to present the indoor characterization of the GOCRSH concentrators under standard test conditions (STCs) which have never been tested before. The chosen concentrators are GOCRSH_A, GOCRSH_B, GOCRSH_C_{rh} and GOCRSH_D.

Section 2 describes the GOCRSH prototype fabrication and assembly process. Section 3 outlines the indoor experimental setup while Section 4 presents the results and discussions. The conclusions are provided in Section 5.

2. GOCRSH prototype fabrication and assembly

2.1 Prototype components

The process to create a GOCRSH concentrator has been explained in detail by Freier Raine et al. (2020). Specifically for the test, four type of GOCRSH concentrators were fabricated. The detailed characteristics and parameters of these concentrators are presented in Table 1. Figure 1 demonstrated the side profile parameters of GOCRSH entrance aperture profile and hyperbolic side profile.

Table 1. Characteristics and parameters of the chosen GOCRSH designs.

	Lens	GOCRSH_A	GOCRSH_B	GOCRSH_C_{rh}	GOCRSH_D
Characteristics	Volume V in mm^3	2696	2285	3796	3079
	Optical concentration gain $C_{opt\pm40°}$	2.91	2.75	3.36	3.01
	Maximum concentrator height h_m in mm	12.74	11.74	16.64	13.16
	Entrance aperture diameter d_E in mm	21.79	20.62	22.01	22.77
	Geometrical concentration gain C_g	3.73	3.34	3.80	4.07
	Optical efficiency $\eta_{opt\pm40°}$	0.77	0.81	0.88	0.73
Parameters	*Re* in mm	11.4856	10.6031	11.0033	11.6638
	Circle centre x-coordinate of the arc x_c in mm	- 0.2034	- 0.0041	0	- 0.0128
	Circle centre y-coordinate of the arc y_c in mm	- 2.9517	- 2.4546	0	- 2.4835
	Side Profile Height h_P in mm	4.2055	3.5909	6.6435	3.9837

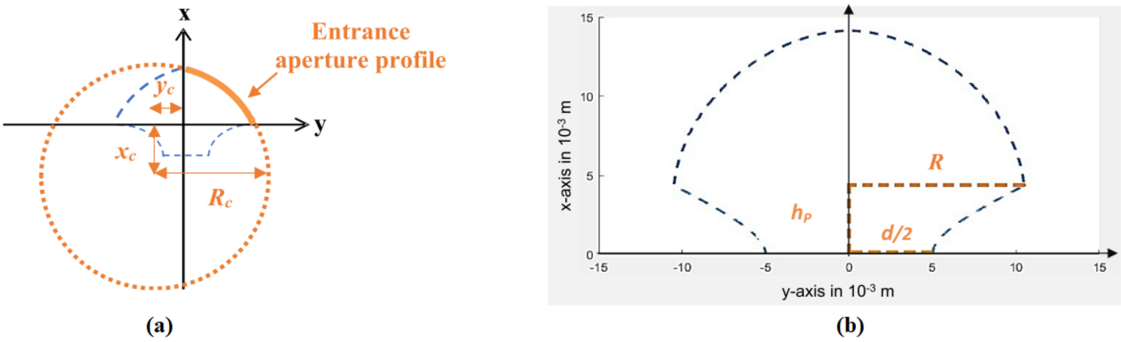

Figure 1: Parameters of the GOCRSH (a) entrance aperture profile, side view, and (b) hyperbolic side profile.

The GOCRSH prototypes were CNC machined from transparent PMMA since CNC machining is more cost effective for prototyping than injection moulding (Abu-Bakar, 2016). The GOCRSH prototypes were machined and hand-polished by Dongguan Bole RP&M Co Ltd according to the IGES files provided to the company. The CNC machined and hand polished GOCRSH concentrator prototypes are shown in Figure 2. The PMMA material was chosen due to its durability. Mahoney et al. (1993) has carried out an accelerated UV test on several PMMA materials commonly used for PV systems. They found that PMMA has an excellent durability, losing only 2% of solar averaged hemispherical transmittance after being aged for 36.5 years.

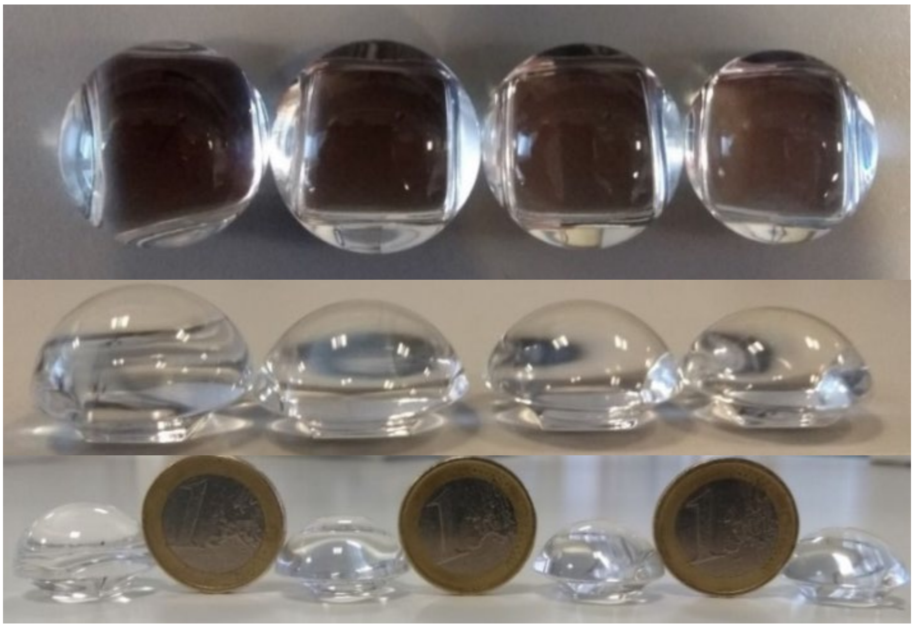

Figure 2. Concentrator prototypes from left to right: GOCRSH_C_{rh}, GOCRSH_D, GOCRSH_A and GOCRSH_B.

To fabricate the GOCRSH concentrator devices, laser grooved buried contact (LGBC) PV cells from Solar Capture Ltd were used since they were available within the university. These cells are designed for CPV applications with concentration ratios below 10x. The measured solar cell size is 100 mm^2 including the area allocated for the front contact. This means that for a concentrator with a 100 mm^2 square exit aperture, a part of the light rays will be focused onto the tabbing wire and consequently be lost due to reflection. A cell efficiency of only 10% was determined experimentally under STC conditions for an active cell area of 100 mm^2.

2.2 Photovoltaic cell tabbing process

For the tabbing of the cells a flat lead-free wire of 0.1 mm thickness and 1 mm width was cut into small pieces of approximately 150 mm length. For a better bonding between the solar cell and the tabbing wire, one side of the tabbing wire and the back contact of the solar cell were covered with liquid flux. A small amount of solder was applied onto the cleaned and fluxed side of the tabbing wire with an 81 W soldering iron at a working temperature of 350°C. To create a connection, heat was applied onto the tabbing wire which was positioned with the applied solder touching the back contact of the cell. The tabbing process was repeated for the front contact of the cell. The tabbed cell was attached to a 60 mm x 60 mm x 4 mm glass substrate with a drop of superglue; just enough to create a connection without overflowing the sides of the cell. Five solar cells in total were tabbed to create four GOCSRH concentrating devices and a reference cell device. All cells were tested under the solar simulator before the prototypes were assembled and a short circuit current of around 25 mA was obtained under STCs for all cells using a multimeter.

2.3 Assembly process

A silicon elastomer Sylgard-184 from Dow Corning was used to attach the concentrators to the solar cells. Sylgard-184 is an adhesive, encapsulant and index matching gel for solar cells with further applications being the protection of electrical/electronic devices and potting applications (Dow Corning, 2017). Sylgard-184 is a two-part adhesive which was mixed by weight in a ratio of 10 parts base to 1 part of curing agent. The mixture was thoroughly stirred in a beaker and since the stirring entraps air, the mixture was placed in a vacuum chamber for 10-15 minutes under 400 mbar until all visible air bubbles evaporated. Before the Sylgard-184 was applied, the cells were brushed with a liquid primer (Dow Corning Primer 92-023) to improve the adhesion between the silicon elastomer and the solar cell using a soft brush. The primer is a harmful and corrosive material and should be treated with caution (Dow, 2018). The primer and the elastomer were handled under the fume hood wearing protective clothing, gloves and glasses. Creating a thin coating, the elastomer was applied onto the solar cell and the glass around it to create a large surface area between the cell, the adhesive and the substrate.

Extra care was taken to reduce misalignment and the entrapment of air bubbles between the solar cell and the concentrator. Since the tabbed back- and front-contact were situated on the same side of the cell, the tabbing wires lead to a tilt of the concentrator when placed on the cell. To prevent the concentrator sliding off the cell during the curing period, a paper was placed underneath the one side of the substrate to level the concentrator (Figure 3). The samples were left to cure at room temperature under the fume hood for 48 hours.

Figure 3. Attachment of the concentrators.

3. Experimental setup

The experimental analysis was carried out indoors under an Oriel® Sol3A™ Class AAA solar simulator. The xenon short arc lamp of an AAA class solar simulator is ozone free and has a spectral performance match between 0.75 to 1.25 times of a 5800 K blackbody. Both the temporal instability and the non-uniformity of the irradiance are less than 2% within a 200 mm by 200 mm footprint at a working distance of 365-395 mm. The irradiance is adjustable between 0.1 and 1 suns where 1 sun equals to 1000 W/m^2. Furthermore, the Oriel® Sol3A™ Class AAA solar simulator has an integrated 1.5 AM filter to enable STC experimental conditions (Zeiny et al., 2018). The experiment setup is shown in Figure 4.

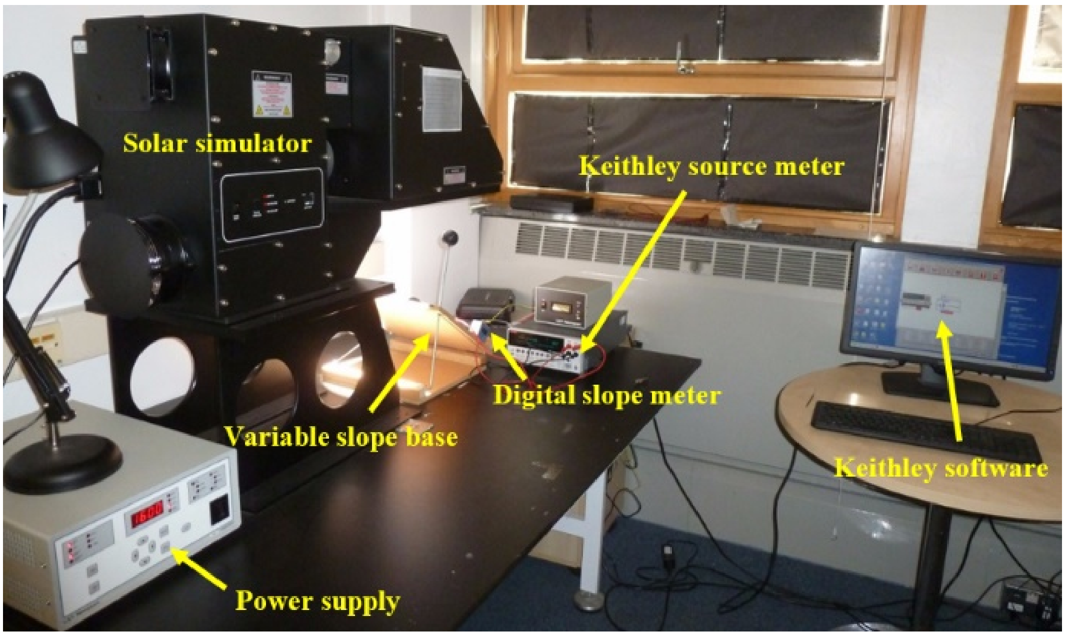

Figure 4. Setup of the indoor experiment.

A SourceMeter instrument from Keithley Instruments (model 2440 5A) was used in combination with the Keithley LabTracer 2.0 software for *I-V* curve tracing. The SourceMeter is a highly stable multimeter which can be used either as a voltage/current source or a voltage/current/resistance meter. The SourceMeter transmits 1700 readings per second and the readings are taken using a four-wire set up which is more accurate than a two-wire set up (Keithley Instruments Inc, 2016). The irradiance of the solar simulator was set to 1000 W/m^2 according to STC and was controlled during the experiment with an Oriel PV Reference Cell System (Model 91150V). The reference cell consists of a 400 mm^2 mono-c-Si solar cell and a type K thermocouple. Thus, the sun irradiance and the cell temperature can be measured simultaneously. When not placed under the solar simulator, the reference cell can be used to measure the room temperature.

4. Results and discussion

4.1 Characterization of the GOCRSH at normal incidence under STCs

I-V and *P-V* curves of the non-concentrating and concentrating devices were measured at normal incidence to show the differences in short-circuit current I_{sc}, open-circuit voltage V_{oc} and maximum power point P_{MPP}. The *I-V* curve tracer was set to sweep the voltage from 0.1 V to 1 V to provide the *I-V* curve of the cell consisting of 100 points. The *I-V* curves of the concentrated cells and the reference cell are shown in Figure 5(a) and the *P-V* curves in Figure 5(b). The P_{MPP}, the cell efficiency (η_{cell}) and the fill-factor (*FF)* of the concentrating and non-concentrating devices were calculated from the traced *I-V* curves and are compared in Table 2.

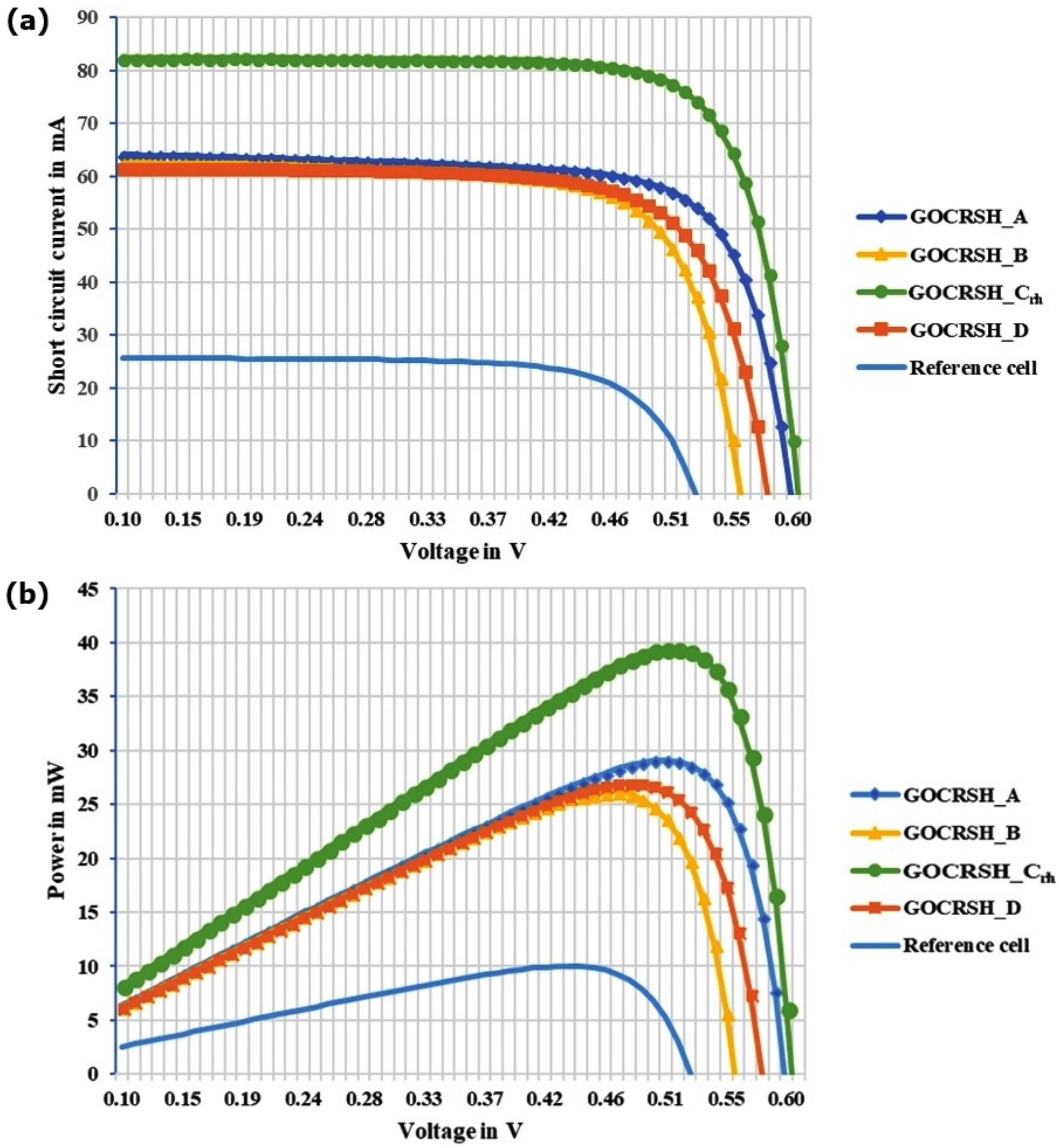

Figure 5. (a) *I-V* curves and (b) *P-V* curves of the GOCRSH concentrated cells and the reference cell under STC conditions

Table 2. Electrical characteristics of the GOCRSH concentrated cells and the reference cell

	Reference cell	**GOCRSH_A**	**GOCRSH_B**	**GOCRSH_C$_{rh}$**	**GOCRSH_D**
I_{sc} in mA	25.54	64.00	62.50	82.40	61.69
V_{oc} in V	0.53	0.60	0.56	0.60	0.58
P_{MMP} in mW	10.02	29.10	26.20	39.47	26.94
FF	0.74	0.76	0.75	0.80	0.75
η_{cell}	0.10	0.29	0.26	0.39	0.27

The power factor and thus the increase in cell efficiency is as high as 3.9x times for the GOCRSH_C$_{rh}$ and 2.9x, 2.6x and 2.7x for the concentrators GOCRSH_A, GOCRSH_B and GOCRSH_D respectively. The power factor is greater than the short circuit current factor since it also includes the logarithmically proportional increase in the maximum power point voltage (Quaschning, 2015).

The opto-electronic concentration ratio ($C_{opt\text{-}el}$) of the GOCRSH concentrators at normal incidence (0º inclination) were calculated and are compared to the optical concentration ratio obtained from simulations in Table 3. The opto-electronic concentration ratio is defined as the ratio of I_{sc} with the concentrator and I_{sc} without the concentrator. It can be observed that the experimentally determined $C_{opt\text{-}el}$ is distinctively lower than the simulated optical concentration ratio C_{opt} showing an error greater than 12% for the GOCRSH_A, GOCRSH_B and GOCRSH_D and an error smaller than 5% for the GOCRSH_C$_{rh}$. Before discussing the possible reasons for the obtained errors, the simulated and experimentally obtained angular response are compared in the following section.

Table 3. Comparison of the simulated optical concentration ratio (C_{opt}) and experimentally determined opto-electronic concentration ratio ($C_{opt\text{-}el}$) at normal incidence

	GOCRSH_A	**GOCRSH_B**	**GOCRSH_C$_{rh}$**	**GOCRSH_D**
$C_{opt\_0°}$	2.90	2.75	3.39	3.05
$C_{opt\text{-}el\_0°}$	2.51	2.40	3.22	2.45
Error in %	**13.5**	**12.7**	**5.0**	**16.7**

4.2 Angular response of the GOCRSH under STCs

To determine the angular response of the GOCRSH, the *I-V* curves of the prototypes and the reference cell were measured at various angles of incidence of up to ± 70° in increments of 5°. A variable slope was used to tilt the device and the inclination was measured by a digital tilt meter. The irradiance was set to 1000 W/m^2 and the room temperature was maintained at 25°C. For the first set of the experiments the solar cell was positioned with the tabbing wire facing up on the variable slope (see Figure 6 (a)). However, the tabbing wire in that position can introduce a shade at larger angles of incidence, the experiments were therefore repeated with the tabbing wire at the side (see Figure 6(b)). The results are presented in Figures 7 to 10.The experimental results are compared to each other and to the simulation results in Figures 7 to 10 for each of the GOCRSH prototypes individually.

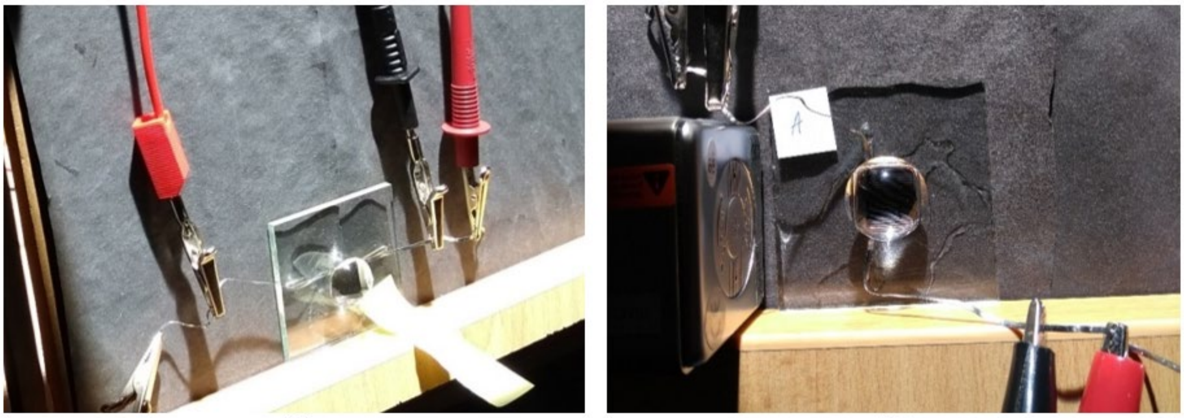

(a) (b)

Figure 6. Measuring the angular acceptance, experimental setup with:
(a) tabbing wire on the top, (b) tabbing wire on the side

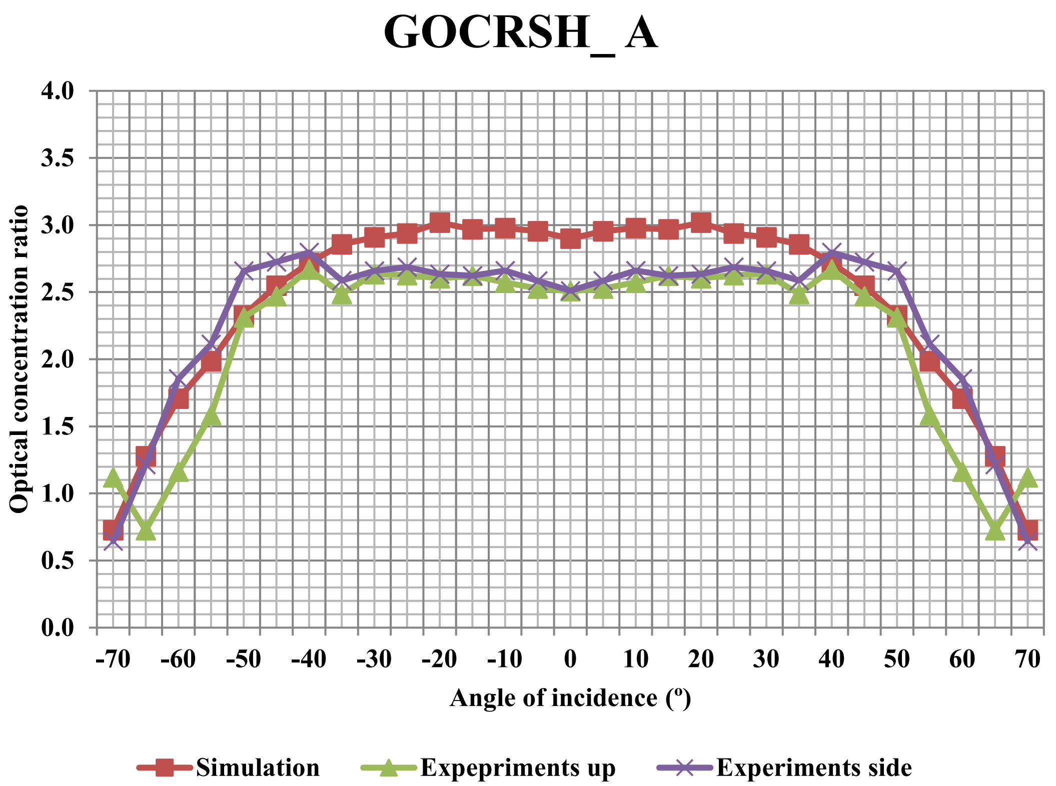

Figure 7. Experimental and simulated angular acceptance of the GOCRSH_A concentrator

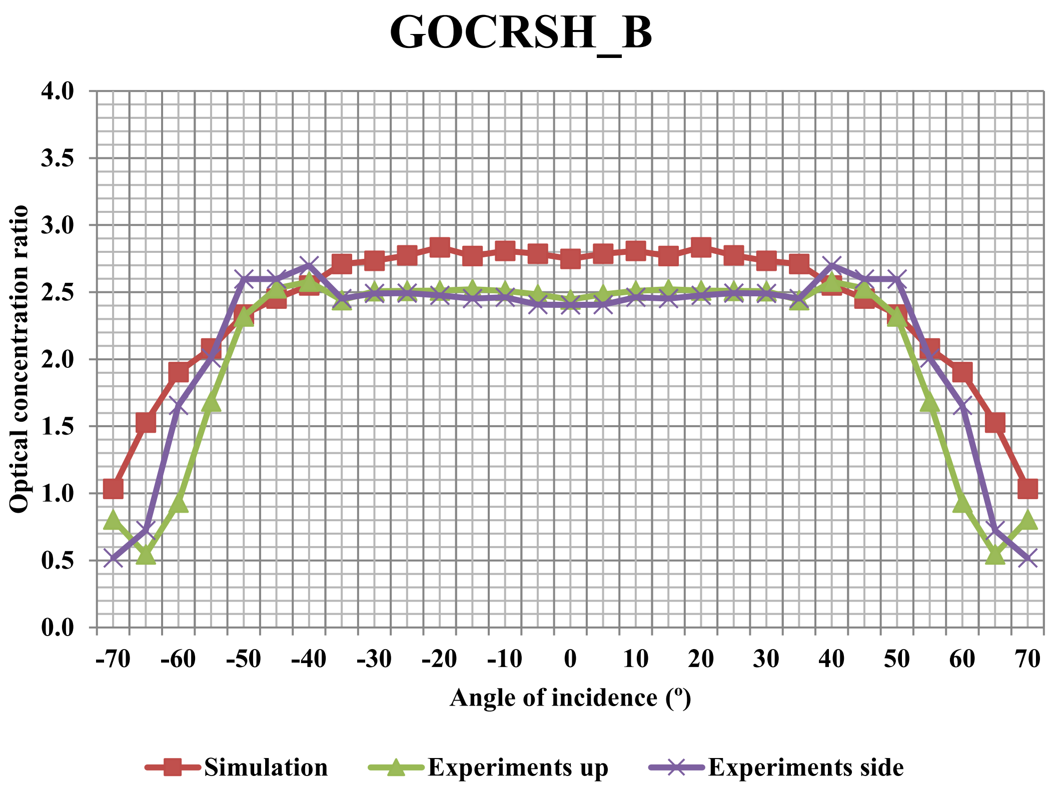

Figure 8. Experimental and simulated angular acceptance of the GOCRSH_B concentrator

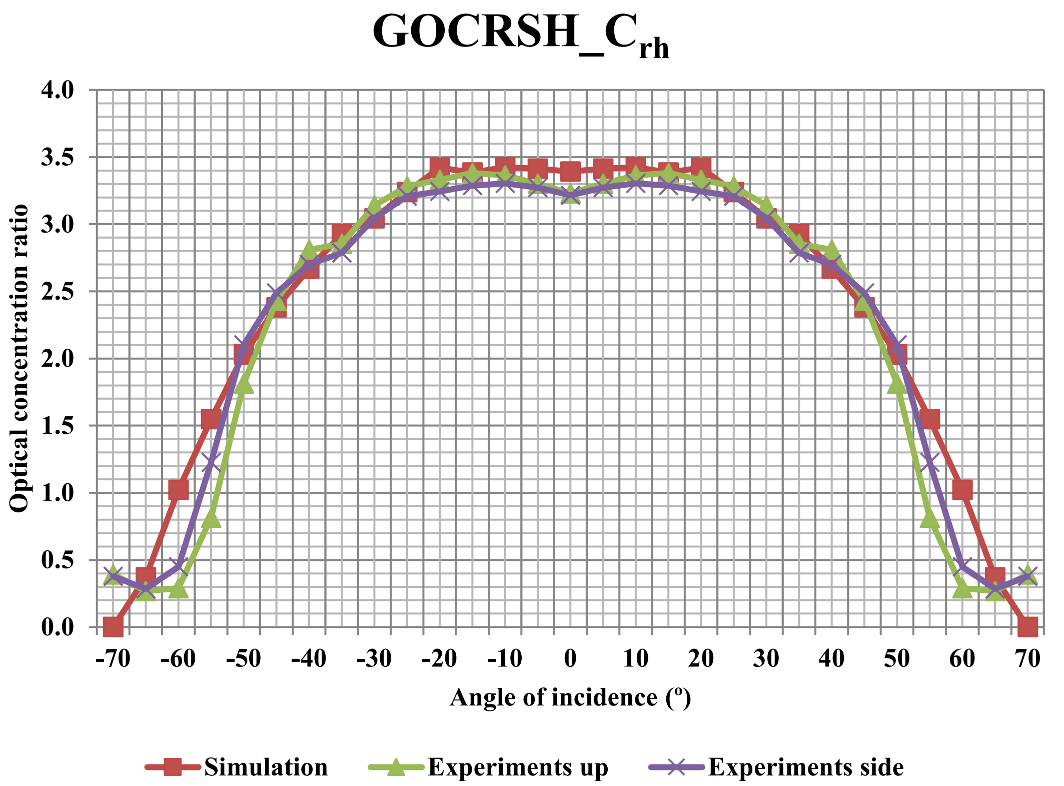

Figure 9. Experimental and simulated angular acceptance of the GOCRSH_C$_{rh}$ concentrator

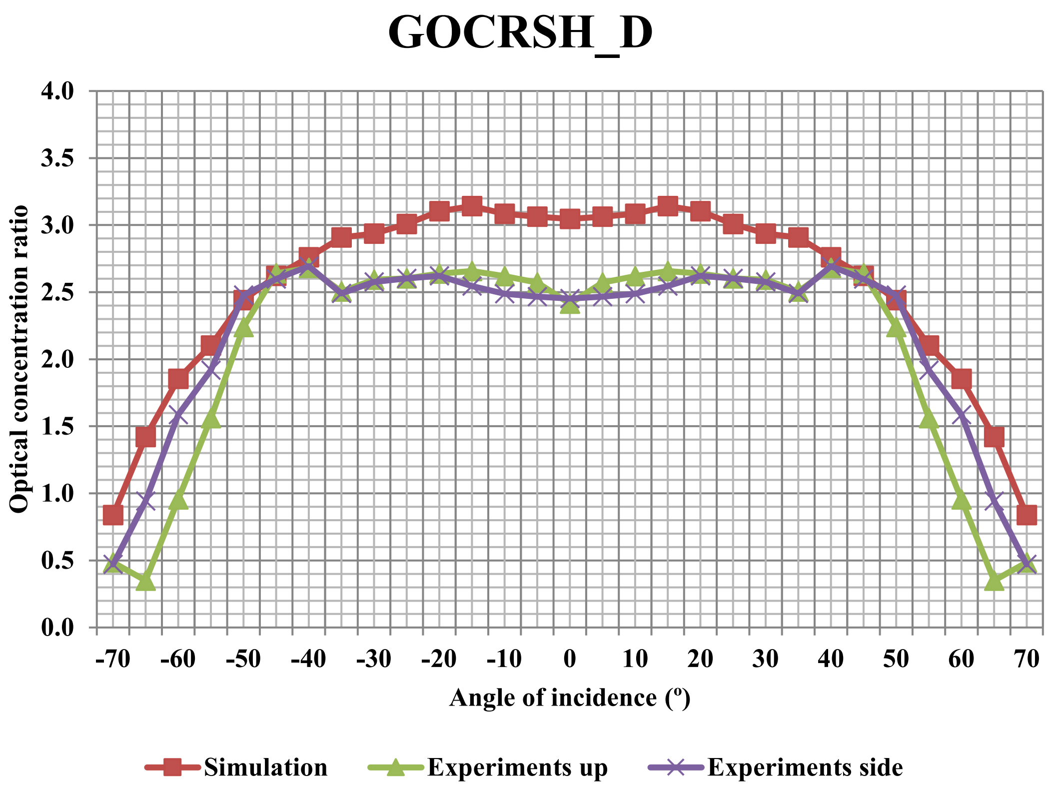

Figure 10. Experimental and simulated angular acceptance of the GOCRSH_D concentrator

Based on the experimental values, the GOCRSH_A, GOCRSH_B, and GOCRSH_D exhibited a general trend. It was observed that the opto-electronic concentration ratios between the angle of incidence of ±35˚ were almost constant at a specific value. The opto-electronic concentration ratio then experienced a peak at ±40˚, before slowly decreasing when the angle of incidence was increased up to ±50˚. Beyond ±50˚, the opto-electronic concentration ratio suffered a gradual drop, to less than 1 at the angle of incidence of ±65˚.

For the GOCRSH_C_{rh}, its opto-electronic concentration ratios remain almost constant between the angles of incidence of ±25˚ at around 3.2. The opto-electronic concentration ratio then slowly decreasing when the angle of incidence was increased up to ±40˚. Beyond ±40˚, the opto-electronic concentration ratio suffered a gradual drop, to less than 1 at the angle of incidence of ±60˚.

Comparing the angular acceptance obtained in the experiments with the tabbing wire on the side to the results with the tabbing wire on the top, it can be seen that more light reaches the solar cell at angles greater ± 40º when the tabbing wire is on the side. This is due to the tabbing wire introducing a shade on the solar cell when placed on top.

Comparing the simulated and experimentally obtained optical efficiencies we can see that there is a high mismatch between $C_{opt\pm40^o}$ and $C_{opt\text{-}el\pm40^o}$ for the concentrators GOCSRH_A, GOCSRH_B and GOCSRH_D (Table 4). While manufacturing errors were expected to lead to a lower $C_{opt\text{-}el\pm40^o}$ compared to $C_{opt\pm40^o}$, a mismatch of 9% and greater is not within the expected norm. This is possibly due to prototype manufacturing, device assembly and experiment errors.

Table 4. Comparison of the simulation and experimental results

	GOCRSH_A	**GOCRSH_B**	**GOCRSH_C_{rh}**	**GOCRSH_D**
$C_{opt\pm40^o}$	2.91	2.75	3.21	3.01
$C_{opt\text{-}el\pm40^o}$ tabbing wire on top	2.58	2.50	3.19	2.59
Error in %	**11.34**	**9.00**	**0.62**	**13.95**
$C_{opt\text{-}el\pm40^o}$ tabbing wire on side	2.64	2.48	3.12	2.55
Error in %	**9.28**	**9.82**	**2.80**	**15.28**

Since the GOCRSH_C_{rh} has by far the smallest error between $C_{opt\text{-}el\pm40^o}$ and $C_{opt\pm40^o}$, the main error must be due to the reflection caused by the entrapped material on the solar cell (Figures 7-14). When seen from the top, the bubbles are transparent and show reflective behaviour at certain angles. It is therefore assumed that the reflections are entrapped air bubbles. However, the pattern of the bubbles shown in Figure 11 give the impression of a brushed liquid. In fact, the primer on the GOCRSH_A, GOCSRH_B and GOCRSH_D PV cells was left to dry longer than on the GOCRSH_C_{rh} PV cell. The primer left to dry too longer might have caused the impurities on the GOCRSH_A, GOCSRH_B and GOCRSH_D cells.

A further source of error are rays which are focused onto the tabbing wire and reflected back. This can be best observed in the angular response of the GOCRSH_C_{rh}, since the focused light beam print on the GOCRSH_C_{rh} concentrated cell is narrower. At normal incidence the optical concentration ratios for both cases, when the tabbing wire is on the side and on top are the same. The optical concentration ratios obtained when the tabbing wire was on top however are slightly higher for the angles of incidence between 5° and 45°. This is because with an increasing angle of incidence, the focused light beam is moving away from the tabbing wire when the tabbing wire is placed on top, making ray losses from reflection from the tabbing wire less significant. For the GOCRSH_A, GOCRSH_B and GOCRSH_D the difference is not as pronounced since the focused light beam prints on the GOCRSH_A, GOCRSH_B and GOCRSH_D concentrated cells are larger.

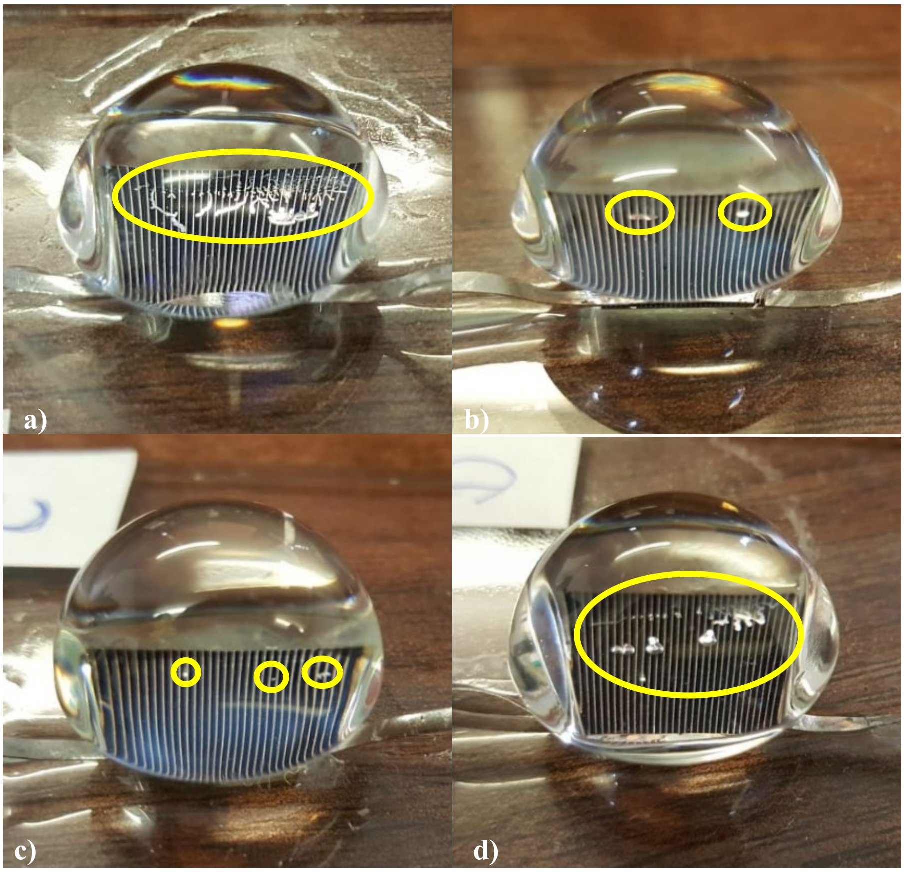

Figure 11. Integration errors due to air entrapment
a) GOCRSH_A, b) GOCRSH_B, c) GOCRSH_C$_{rh}$, d) GOCSRH_D

A further source of errors is the tilt of the concentrator on the solar cell. This is due to the tabbing wire being positioned on the front and the back contact of the cell at the same cell side. Thus, on one side of the cell, the position of the concentrator was 0.2-0.3 mm higher than on the other side (Figure 12). Furthermore, a misalignment of the concentrators and on the solar cells leads to ray losses. Whilst a slight misalignment can be seen between the GOCRSH_C$_{rh}$ and the solar cell (Figure 13), less visible misalignments of the other concentrators are possible. Further possible errors include: soldering errors, error in the 3D model created from MATLAB coordinates, error introduced during the CNC machining and polishing of the prototype, positioning error of the device on the variable slope during the experimental analysis and precision error of the used measuring devices.

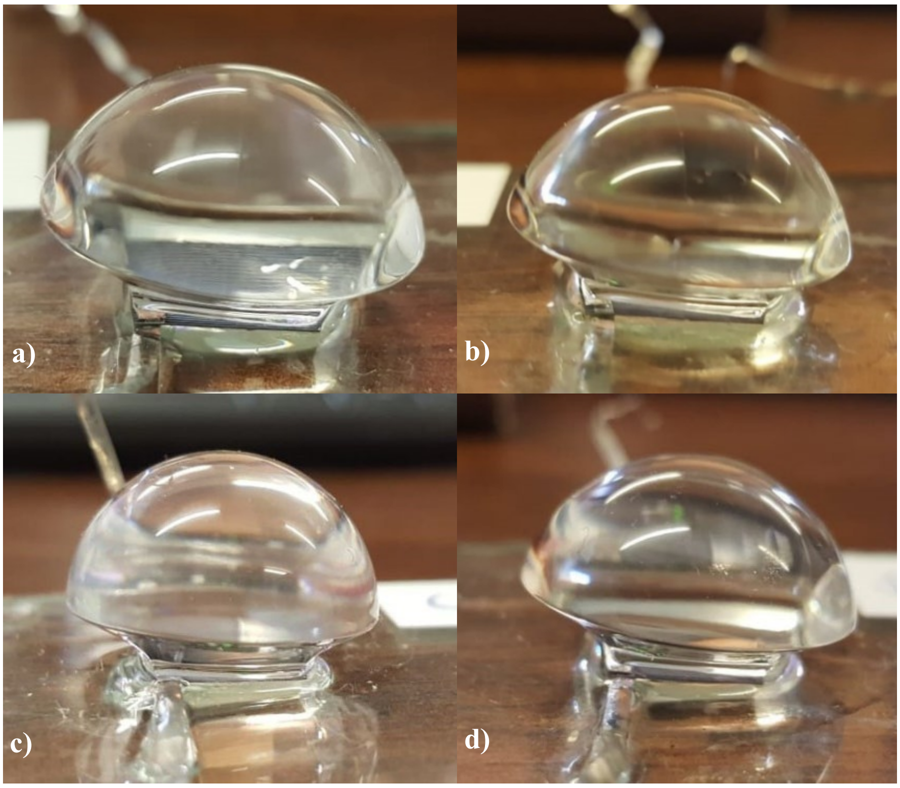

Figure 12. Integration errors due to the tilt of the GOCRSH concentrators
a) GOCRSH_A, b) GOCRSH_B, c) GOCRSH_C, d) GOCSRH_D

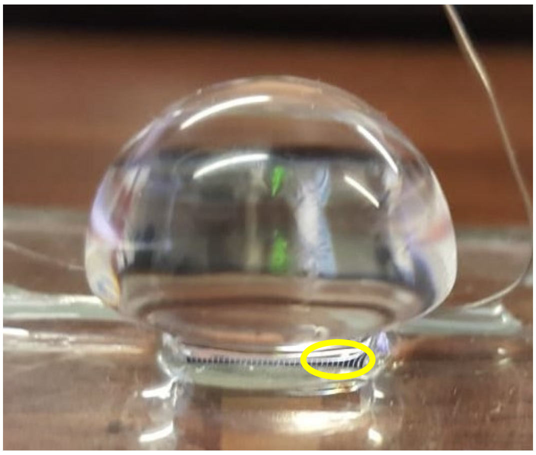

Figure 13. Integration errors due to misalignment between the concentrator and the cell

4.3 Thermal characteristics of the GOCSRH

When exposed to sunlight over a period of time, the temperature of the solar cell increases. This is due to the difference in the energy of the absorbed photons and the photogenerated electrons being emitted in the form of heat in the PV material. An increase in irradiance leads to more absorbed photons and thus to more thermal losses. An increase in cell temperature however, has a negative impact on the cell performance.

For the thermal analysis, the GOCRSH_A concentrating device was chosen as a representation of the GOCSRH designs due to the opto-electronic concentration ratio at normal incidence being similar for GOCRSH_A, GOCRSH_B and GOCRSH_D. A concentrator with an opto-electronic concentration ratio of around 3.0x (RACPC) and a concentrator with an opto-electronic concentration ratio of around 3.3x were tested for their thermal performance by Abu-Bakar et al. (2015) and Sellami (2013) respectively. Whilst the increase in temperature on the cell also depends on the flux distribution on the solar cell and on the point of measurement, the results obtained by Abu-Bakar et al. (2015) and Sellami (2013) can be taken as a guide for the GOCRSH_C_{rh}.

During the experiment the irradiance was set to 1000 W/m^2 and the room temperature was maintained at 25 ºC. Since it is not possible to attach the thermocouple directly to the cell, a type K thermocouple was attached to the glass substrate at the back-side of the cell at and the cell temperature was measured via an ammeter. Although glass has a low thermal transmission of between 0.76 – 1 W/mK (Schott Advanced Optics, 2018; Tafakkori and Fattahi, 2021), this test arrangement was verified by a 3D heat transfer model by Sellami (2013).

The room temperature, cell temperature and the *I-V* curve of the solar cell were recorded every 15 min over a period of 4.5 hours. The temperature settled at around 54.2 ºC after 3 hours (Table 5). The maximum power (P_{MMP}) of the GOCRSH_A concentrating device reduced from 26.41 mW to 23.47 mW, which is a total of 10.8%. Comparatively, a maximum temperature of the solar cell of 57 ºC and a 13.7% reduction in power were recorded with the RACPC (Abu-Bakar et al., 2015), whilst for the H3 SEH a maximum temperature of 56.25°C and a 13.4% power reduction were recorded (Sellami, 2013). Thus, a similar reduction in power can be assumed for the GOCRSH_C_{rh} due to its similar opto-electronic concentration ratio at normal incidence as the RACPC and the H3 SEH. Table 5 shows the change in temperature and P_{MMP} of the GOCRSH_A cell over time. However, it can be seen that the reduction of maximum power of GOCRSH_A was the lowest when compared with the RACPC and SEH concentrator under the same experimental setting.

The temperature coefficient for the maximum power, the maximum voltage and the maximum current of the GOCRSH_A cell were determined based on these results. These values were calculated by determining the ratio of change in each parameter with respect to the change in temperature (Abu-Bakar et al., 2015; Mammo et al., 2013). It was found that the maximum power coefficient was -0.0963 mW/°C, the maximum voltage coefficient was -0.0017 mV/°C and the maximum current coefficient was -0.02 mA/°C.

Table 5. Variation of the maximum power in relation to the change in cell temperature

Time in h	**Room temperature in ºC**	**Cell temperature in ºC**	I_{sc} **in mA**	V_{oc} **in V**	P_{MPP} **in mW**	***FF***	**Efficiency**
0.00	24.54	25.00	59.01	0.60	26.41	0.75	0.26
0.25	24.53	38.40	58.00	0.58	25.07	0.74	0.25
0.50	25.04	47.10	58.20	0.56	24.28	0.74	0.24
0.75	25.07	50.10	58.69	0.55	23.93	0.74	0.24
1.00	25.11	50.90	58.64	0.55	24.03	0.74	0.24
1.25	25.37	52.60	58.59	0.55	23.86	0.73	0.24
1.50	25.30	53.00	58.50	0.55	23.76	0.74	0.24
1.75	25.00	52.80	58.47	0.55	23.81	0.73	0.24
2.00	25.20	53.20	58.45	0.55	23.75	0.74	0.24
2.25	24.97	53.00	58.38	0.55	23.75	0.75	0.24
2.50	25.14	53.60	58.44	0.55	23.70	0.74	0.24
2.75	25.15	53.60	58.51	0.55	23.77	0.74	0.24
3.00	25.23	54.20	58.49	0.55	23.70	0.74	0.24
3.25	25.26	53.80	58.51	0.55	23.80	0.73	0.24
3.50	25.16	54.20	58.44	0.55	23.59	0.74	0.24
3.75	25.63	54.40	58.53	0.55	23.58	0.74	0.24
4.00	25.47	54.20	58.53	0.55	23.70	0.74	0.24
4.25	25.18	55.20	58.43	0.55	23.47	0.74	0.23
4.50	25.33	54.50	58.42	0.55	23.57	0.74	0.24

5. Summary and conclusions

Energy services are vital to inhibiting the COVID-19 pandemic especially in developing countries. Solar energy can be harnessed for use in those countries and one way to do it is by using CPV technology. This technology has been shown to lessen the impact on the environment by substituting part of the PV material with solar PV concentrators. There are numerous concentrator designs developed by researchers and one of them is the GOCRSH concentrator.

In this paper, the experimental analysis of the GOCRSH_A GOCRSH_B, GOCRSH_C_{rh} and GOCRSH_D was carried out. Firstly, the assembly process of the prototypes was described. Secondly, the prototypes were analysed indoors under the solar simulator showing an opto-electronic concentration ratio of 2.90x, 2.75x, 3.39x, 3.05x under normal incidence and 2.51x, 2.4x, 3.22x, 2.45x when averaged for the angular range of ± 40º the GOCRSH_A GOCRSH_B, GOCRSH_C_{rh} and GOCRSH_D respectively. A P_{MPP} ratio under normal incidence of 2.9x, 2.6x, 3.9x and 2.7x was observed with the GOCRSH_A GOCRSH_B, GOCRSH_C_{rh} and GOCRSH_D respectively.

Compared to the $C_{opt\_0^o}$ values obtained from the simulation analysis, the experimentally determined $C_{opt-el\_0^o}$ showed a smaller concentration ratio by 13.5%, 12.7%, 5.0% and 16.7% for the GOCRSH_A GOCRSH_B, GOCRSH_C_{rh} and GOCRSH_D respectively. The mismatch between the average $C_{opt-el\pm40^o}$ and the average $C_{opt\pm40^o}$ was found to be lower than the mismatch between the $C_{opt\_0^o}$ and $C_{opt-el\_0^o}$ values.

The large mismatch between the simulation and experimental results was identified to be due to several manufacturing errors, including entrapped air bubbles on the solar cell, a smaller active area of the cell than the exit aperture of the GOCRSH and the tilt of the concentrators on the cell. Since GOCRSH_C_{rh} showed the smallest error, the main cause for the high mismatch values was assumed to be due to the entrapped air on the solar cells, which have been observed mainly for the GOCRSH_A GOCRSH_B and GOCRSH_D concentrating devices.

Furthermore, the effect of temperature increase on the solar cell performance was measured for the GOCRSH_A under constant illumination for 4.5 hours. A maximum temperature of 54º and a power decrease of 10.7% were recorded, similar to the power decrease of BICPV concentrators described in literature.

Based on the indoor characterizations, it can be concluded that the GOCRSH CPV has the capability to be used as an alternative power source in developing countries. However, to ensure that the design can achieve optimum performance, it is necessary to minimize the errors especially during the manufacturing stage. Moreover, the design must also incorporate a suitable cooling system to minimize the rise in temperature during its operation.

CRediT authorship contribution statement

Daria Freier Raine: Conceptualization, Methodology, Software, Writing - original draft, Visualization, Investigation, Writing - Review & Editing. **Firdaus Muhammad-Sukki:** Supervision, Writing - original draft, Writing - Review & Editing. **Roberto Ramirez- Iniguez:** Supervision, Methodology, Funding acquisition, Writing - Review & Editing. **Tahseen Jafry:** Supervision. **Carlos Gamio:** Supervision, Methodology

Acknowledgement

The authors would like to thank Glasgow Caledonian University for funding the research activity.

References

Abu-Bakar, S.H., 2016. Novel Rotationally Asymmetrical Solar Concentrator for the Building Integrated Photovoltaic System. PhD Thesis, Glasgow Caledonian University, United Kingdom.

Abu-Bakar, S.H., Muhammad-Sukki, F., Freier, D., Ramirez-Iniguez, R., Mallick, T.K., Munir, A.B., Mohd Yasin, S.H., Abubakar Mas'ud, A., Md Yunus, N., 2015. Performance analysis of a novel rotationally asymmetrical compound parabolic concentrator. Appl. Energy 154, 221–231. https://doi.org/10.1016/j.apenergy.2015.04.122

Abubakar Mas'ud, A., Wirba, A.V., Muhammad-Sukki, F., Albarracín, R., Abu-Bakar, S.H., Munir, A.B., Bani, N.A., 2016. A review on the recent progress made on solar photovoltaic in selected countries of sub-Saharan Africa. Renew. Sustain. Energy Rev. 62, 441–452. https://doi.org/10.1016/j.rser.2016.04.055

Avila, N., Carvallo, J.P., Shaw, B., Kammen, D.M., 2017. The energy challenge in sub-Saharan Africa: A guide for advocates and policy makers - Part 1: Generating energy for sustainable and equitable development. Boston, Massachusetts, USA.

Baig, H., Kanda, H., Asiri, A.M., Nazeeruddin, M.K., Mallick, T., 2020. Increasing efficiency of perovskite solar cells using low concentrating photovoltaic systems. Sustain. Energy Fuels 4, 528–537. https://doi.org/10.1039/c9se00550a

Beuse, M., Dirksmeier, M., Steffen, B., Schmidt, T.S., 2020. Profitability of commercial and industrial photovoltaics and battery projects in South-East-Asia. Appl. Energy 271, 115218. https://doi.org/10.1016/j.apenergy.2020.115218

Burke, P.J., Widnyana, J., Anjum, Z., Aisbett, E., Resosudarmo, B., Baldwin, K.G.H., 2019. Overcoming barriers to solar and wind energy adoption in two Asian giants: India and Indonesia. Energy Policy 132, 1216–1228. https://doi.org/10.1016/j.enpol.2019.05.055

Cvijovic, D., Klinowski, J., 2002. Taboo search: An approach to the multipleminima problem for continuous functions, in: Pardalos, P.M., Romeijin, H.. (Eds.), Handbook of Global

Optimization. Kluwer Academic Publishers, pp. 387–406.

Dow, 2018. DOWSIL 92-023 Primer, Safety Data Sheet. Derbyshire, England.

Dow Corning, 2017. Technical Data Sheet: Sylgard 184 Silicone Elastomer. Midland, Michigan, USA.

Elminshawy, N.A.S., El-Ghandour, M., Elhenawy, Y., Bassyouni, M., El-Damhogi, D.G., Addas, M.F., 2019. Experimental investigation of a V-trough PV concentrator integrated with a buried water heat exchanger cooling system. Sol. Energy 193, 706–714. https://doi.org/10.1016/j.solener.2019.10.013

Foster, S., Muhammad-Sukki, F., Ramirez-Iniguez, R., Raine, D.F., Deciga-Gusi, J., Abu-Bakar, S.H., Bani, N.A., Munir, A.B., Mas'ud, A.A., Ardila-Rey, J.A., 2020. Assessment of the RACPC performance under diffuse radiation for use in BIPV system. Appl. Sci. 10, 3552:1–11. https://doi.org/10.3390/APP10103552

Fraunhofer Institute for Solar Energy Systems, 2018. Photovoltaics Report. München, Germany.

Freier, D., Ramirez-Iniguez, R., Gamio, C., Jafry, T., Muhammad-Sukki, F., 2017. Novel nonimaging solar concentrator for portable solar systems for developing countries, in: 2017 IEEE PES PowerAfrica. IEEE, pp. 307–310. https://doi.org/10.1109/PowerAfrica.2017.7991242

Freier Raine, D., Ramirez-Iniguez, R., Jafry, T., Muhammad-Sukki, F., Gamio, C., 2020. Design method of a compact static nonimaging concentrator for portable photovoltaics using parameterisation and numerical optimisation. Appl. Energy 266, 114821:1–12. https://doi.org/10.1016/j.apenergy.2020.114821

Fthenakis, V.M., 2003. Overview of potential hazards, in: Practical Handbook of Photovoltaics: Fundamentals and Applications. New York, pp. 1–856.

Green, M.A., Hishikawa, Y., Dunlop, E.D., Levi, D.H., Hohl-Ebinger, J., Ho-Baillie, A.W.Y., 2018. Solar cell efficiency tables (version 52). Prog. Photovoltaics Res. Appl. 26, 427–436. https://doi.org/10.1002/pip.3040

IEA, 2017. WEO-2017 Special Report: Energy Access Outlook 2017 - Executive Summary. Paris, France.

Keane, J., 2014. Pico-solar Electric Systems. Routledge, New York.

Keithley Instruments Inc, 2016. Series 2400 SourceMeter SMU Instruments. Solon, Ohio, USA.

Kimemia, D., Vermaak, C., Pachauri, S., Rhodes, B., 2014. Burns, scalds and poisonings from household energy use in South Africa: Are the energy poor at greater risk? Energy Sustain. Dev. 18, 1–8. https://doi.org/10.1016/j.esd.2013.11.011

Lamnatou, C., Baig, H., Chemisana, D., Mallick, T.K., 2016. Environmental assessment of a building-integrated linear dielectric-based concentrating photovoltaic according to multiple life-cycle indicators. J. Clean. Prod. 131, 773–784. https://doi.org/10.1016/j.jclepro.2016.04.094

Li, L., Wang, B., Pottas, J., Lipiński, W., 2019. Design of a compound parabolic concentrator for a multi-source high-flux solar simulator. Sol. Energy 183, 805–811. https://doi.org/10.1016/j.solener.2019.03.017

Liu, X., Wu, Y., Hou, X., Liu, H., 2017. Investigation of the optical performance of a novel planar static PV concentrator with Lambertian rear reflectors. Buildings 7, 88. https://doi.org/10.3390/buildings7040088

Mahoney, A.R., Cannon, J.E., Woodworth, J.R., 1993. Accelerated UV-aging of acrylic materials used in PV concentrator systems, in: Conference Record of the IEEE Photovoltaic Specialists Conference. Publ by IEEE, pp. 1216–1221. https://doi.org/10.1109/pvsc.1993.346948

Mammo, E.D., Sellami, N., Mallick, T.K., 2013. Performance analysis of a reflective 3D crossed compound parabolic concentrating photovoltaic system for building façade integration. Prog. Photovoltaics Res. Appl. 21, 1095–1103. https://doi.org/10.1002/pip.2211

Muhammad-Sukki, F., Abu-Bakar, S.H., Ramirez-Iniguez, R., McMeekin, S.G., Stewart, B.G., Sarmah, N., Mallick, T.K., Munir, A.B., Mohd Yasin, S.H., Abdul Rahim, R., 2014. Mirror symmetrical dielectric totally internally reflecting concentrator for building integrated photovoltaic systems. Appl. Energy 113, 32–40. https://doi.org/10.1016/j.apenergy.2013.07.010

Palit, D., 2013. Solar energy programs for rural electrification: Experiences and lessons from South Asia. Energy Sustain. Dev. 17, 270–279. https://doi.org/10.1016/j.esd.2013.01.002

Quaschning, V., 2015. Regenerative Energiesysteme : Technologie - Berechnung - Simulation. Hanser.

Sarmah, N., Richards, B.S., Mallick, T.K., 2014. Design, development and indoor performance analysis of a low concentrating dielectric photovoltaic module. Sol. Energy 103, 390–401. https://doi.org/10.1016/j.solener.2014.02.029

Schott Advanced Optics, 2018. Optisches Glas 2018. Mainz, Germany.

Scott, A., Worrall, L., Hörnberg, J., To, L.S., 2017. How solar household systems contribute to resilience (No. 528), Shaping policy for development. London, UK.

Sellami, N., 2013. Design and Characterisation of a Novel Translucent Solar Concentrator. PhD Thesis, Heriot-Watt University, United Kingdom.

Sharma, M.K., Bhattacharya, J., 2020. A novel stationary concentrator to enhance solar intensity with absorber-only single axis tracking. Renew. Energy 154, 976–985. https://doi.org/10.1016/j.renene.2020.03.064

Tafakkori, R., Fattahi, A., 2021. Introducing novel configurations for double-glazed windows with lower energy loss. Sustain. Energy Technol. Assessments 43, 100919. https://doi.org/10.1016/j.seta.2020.100919

United Nations, 2021. The Sustainable Development Agenda. Available at: https://www.un.org/sustainabledevelopment/development-agenda-retired/ (Accessed April 19, 2021).

United Nations, 2017. Goal 7 : Sustainable Development Knowledge Platform. Available at: https://sustainabledevelopment.un.org/sdg7 (Accessed March 6, 2018).

Vellini, M., Gambini, M., Prattella, V., 2017. Environmental impacts of PV technology throughout the life cycle: Importance of the end-of-life management for Si-panels and CdTe-panels. Energy 138, 1099–1111. https://doi.org/10.1016/j.energy.2017.07.031

Xuan, Q., Li, G., Pei, G., Ji, J., Su, Y., Zhao, B., 2017. Optimization design and performance analysis of a novel asymmetric compound parabolic concentrator with rotation angle for building application. Sol. Energy 158, 808–818.

https://doi.org/10.1016/j.solener.2017.10.029

Yan, D., Xu, H., Lan, J., Zhou, K., Ye, Y., Zhang, J., An, Z., Yeager, K.M., 2019. Solar activity and the westerlies dominate decadal hydroclimatic changes over arid Central Asia. Glob. Planet. Change 173, 53–60. https://doi.org/10.1016/j.gloplacha.2018.12.006

Zeiny, A., Jin, H., Bai, L., Lin, G., Wen, D., 2018. A comparative study of direct absorption nanofluids for solar thermal applications. Sol. Energy 161, 74–82. https://doi.org/10.1016/j.solener.2017.12.037